Published for SISSA by Springer

Received: July 9, 2018
Revised: September 25, 2018
Accepted: October 6, 2018
Published: October 19, 2018

Dark matter casts light on the early Universe

A. Arbey,[a,b,1] **J. Ellis,**[b,c,d] **F. Mahmoudi**[a,b] **and G. Robbins**[a,e]

[a] *Univ. Lyon, Univ. Lyon 1, CNRS/IN2P3, Institut de Physique Nucléaire de Lyon, UMR5822, F-69622 Villeurbanne, France*
[b] *Theoretical Physics Department, CERN, CH-1211 Geneva 23, Switzerland*
[c] *Theoretical Particle Physics and Cosmology Group, Department of Physics, King's College London, London WC2R 2LS, U.K.*
[d] *National Institute of Chemical Physics & Biophysics, Rävala 10, 10143 Tallinn, Estonia*
[e] *Univ. Lyon, Univ. Lyon 1, ENS de Lyon, CNRS, Centre de Recherche Astrophysique de Lyon UMR5574, F-69230 Saint-Genis-Laval, France*

E-mail: alexandre.arbey@ens-lyon.fr, John.Ellis@cern.ch, nazila@cern.ch, glenn.robbins@univ-lyon1.fr

Abstract: We show how knowledge of the cold dark matter (CDM) density can be used, in conjunction with measurements of the parameters of a scenario for beyond the Standard Model (BSM) physics, to provide information about the evolution of the Universe before Big Bang Nucleosynthesis (BBN). As examples of non-standard evolution, we consider models with a scalar field that may decay into BSM particles, and quintessence models. We illustrate our calculations using various supersymmetric models as representatives of classes of BSM scenarios in which the CDM density is either larger or smaller than the observed density when the early Universe is assumed to be radiation-dominated. In the case of a decaying scalar field, we show how the CDM density can constrain the initial scalar density and the reheating temperature after it decays in BSM scenarios that would yield overdense dark matter in standard radiation-dominated cosmology, and how the decays of the scalar field into BSM particles can be constrained in scenarios that would otherwise yield underdense CDM. We also show how the early evolution of the quintessence field can be constrained in BSM scenarios.

Keywords: Beyond Standard Model, Cosmology of Theories beyond the SM, Supersymmetric Standard Model

ArXiv ePrint: 1807.00554

[1] Also Institut Universitaire de France, 103 boulevard Saint-Michel, 75005 Paris, France.

https://doi.org/10.1007/JHEP10(2018)132

Contents

JHEP10(2018)132

1 Introduction

The very early Universe before Big-Bang Nucleosynthesis (BBN) is a little-known cosmological era that should provide the answers to several very important questions, such as the origin of the baryon asymmetry in the Universe — possibly due to leptogenesis, the nature of the electroweak and perhaps other phase transitions, the possibility of grand unification, the mechanism for inflation, etc. Unfortunately, as of today we have no direct observations of the period before recombination at $\sim 1\,\text{eV}$, though some constraints can be set using the abundances of the elements generated during BBN, and the cosmic microwave background (CMB) constrains models of inflation. High-energy colliders such as the Large Hadron Collider (LHC) can probe the state of matter at energies $\sim$GeV and particle interactions at energies $\sim$TeV, but the other properties of the early Universe, such as its expansion rate, are still relatively unconstrained.

In this paper we propose to use understanding of the properties of relic dark matter (DM) particles obtained from particle physics to obtain constraints on the properties of

the very early Universe at temperatures $\sim 10 - 100\,\mathrm{GeV}$, orders of magnitude above the scale of BBN.

For this purpose, we consider an observable linking particle physics and cosmology, namely the DM relic density. We assume that DM is cold, and composed of some type of stable weakly-interacting massive particle (WIMP) that was in thermal equilibrium in the early Universe and subsequently froze out. The cold dark matter density has been measured very precisely by the Planck Collaboration using the CMB and observations of the more recent Universe [1]. The Standard Model (SM) of particle physics does not provide any cold dark matter candidate, but many new physics beyond the SM (BSM) have such candidates. The dark matter relic density can be computed in any given BSM scenario, *under the assumption* that the early Universe was dominated by (SM) radiation, and very strict constraints can be set on the parameters of the BSM scenario using the Planck measurements [2].

The hypothesis of radiation domination in the early Universe is correct at temperatures below $\sim$MeV, as indicated by the constraints from BBN and the CMB [3–5]. However, it is possible that it does not hold at higher temperatures. In particular, many cosmological scenarios, such as late inflation [6–8], dark energy [9–16], a dark fluid [17–19], Higgs inflation [20, 21], late-decaying moduli [22–25], dilatons [26, 27], etc., invoke cosmological scalar fields that may have co-existed with radiation at temperatures $\sim$GeV or TeV. Several studies (see, for example, [28–40]) have shown that such scalar fields could have altered the relic density.

In any given BSM scenario, a deviation of the measured cold dark matter density from a calculation based on measurements of the model parameters and standard radiation-dominated expansion would be a signature of novel phenomena in the very early Universe. One might argue that, if the calculated relic density is different from the measured dark matter density, the corresponding BSM scenario is disfavoured. Here, however, we propose to reverse this argument: if the calculated relic density is different from the measured dark matter density, it could be because of novel phenomena in the early Universe. This orthogonal point of view will become particularly important if new particles are discovered at colliders or in dark matter detection experiments: using dark matter observables, it is not possible to constrain BSM scenarios in isolation, but the constraints have to be applied simultaneously to a combination of BSM and cosmological scenarios.

For this analysis, we study two different realistic cosmological scenarios: the case of a decaying scalar field, e.g., a modulus field, which modifies the energy content of the Universe and also injects entropy or BSM particles, and the case of a quintessence field, which could modify the energy content on its way to fulfilling its original purpose of generating dark energy with negative pressure in the recent Universe.

The rest of this paper is organised as follows. In section 2 we review the standard calculation of relic density. Then, in section 3 we introduce cosmological scalar field scenarios that can impact the relic density calculation, and discuss their possible effects. Next, in section 4 we introduce as illustrations of BSM scenarios a selection of supersymmetric scenarios where the measured relic density can differ from that calculated assuming radiation-dominated expansion. Our results are given in section 5 and our conclusions in section 6.

JHEP10(2018)132

2 Relic density calculation

The relic density calculation is generally performed in the standard cosmological model, in which the expansion rate of the Universe is given by the Friedmann equation. In the early Universe when the radiation density dominates this reduces to:

$$H^2 = \left(\frac{\dot{a}}{a}\right)^2 = \frac{8\pi G}{3}\rho_{\rm rad}\,, \tag{2.1}$$

where a is the cosmological scale factor and H the Hubble parameter. The radiation density reads

$$\rho_{\rm rad}(T) = g_{\rm eff}(T)\frac{\pi^2}{30}T^4\,, \tag{2.2}$$

where $g_{\rm eff}$ is the effective number of degrees of freedom of radiation, which is given by the particle content of the Standard Model and the QCD equation of state (see, for example, [41, 42]).

Assuming that, in a given BSM scenario, only the lightest BSM particle is stable, and constitutes a suitable dark matter candidate that was originally in thermal equilibrium, the number of relic particles is obtained by solving the Boltzmann evolution equation [43, 44]:

$$dn/dt = -3Hn - \langle\sigma_{\rm eff}v\rangle(n^2 - n_{\rm eq}^2)\,, \tag{2.3}$$

where n is the number density of BSM particles, $n_{\rm eq}$ is their equilibrium density, and $\langle\sigma_{\rm eff}v\rangle$ is the thermal average of the annihilation rate of pairs of BSM particles to SM particles.

To define $\langle\sigma_{\rm eff}v\rangle$, it is useful to define first the annihilation rate of BSM particles i and j into SM particles k and l:

$$W_{ij\to kl} = \frac{p_{kl}}{16\pi^2 g_i g_j S_{kl}\sqrt{s}} \sum_{\text{internal d.o.f.}} \int |\mathcal{M}(ij\to kl)|^2\, d\Omega\,, \tag{2.4}$$

where $\mathcal{M}$ is the transition amplitude, s is the centre-of-mass energy squared, g_i is the number of degrees of freedom of the particle i, p_{kl} is the final centre-of-mass momentum, given by

$$p_{kl} = \frac{\left[s-(m_k+m_l)^2\right]^{1/2}\left[s-(m_k-m_l)^2\right]^{1/2}}{2\sqrt{s}}\,, \tag{2.5}$$

and S_{kl} is a symmetry factor equal to 2 for identical final particles and to 1 otherwise.

The thermal average of the effective cross section is given by:

$$\langle\sigma_{\rm eff}v\rangle = \frac{\displaystyle\int_0^\infty dp_{\rm eff}\, p_{\rm eff}^2 W_{\rm eff}(\sqrt{s}) K_1\left(\frac{\sqrt{s}}{T}\right)}{m_{\rm relic}^4 T\left[\displaystyle\sum_i \frac{g_i}{g_{LSP}}\frac{m_i^2}{m_1^2}K_2\left(\frac{m_i}{T}\right)\right]^2}\,, \tag{2.6}$$

where K_1 and K_2 are the modified Bessel functions of the second kind of order 1 and 2 respectively, and $W_{\rm eff}$ is an effective annihilation rate:

$$W_{\rm eff} \equiv \frac{1}{g_{\rm relic}^2 p_{\rm eff}} \sum_{ij} g_i g_j p_{ij} W_{ij}\,, \tag{2.7}$$

JHEP10(2018)132

with

$$p_{\rm eff}(\sqrt{s}) = \frac{1}{2}\sqrt{(\sqrt{s})^2 - 4m_{\rm relic}^2}\,, \tag{2.8}$$

In order to solve the Boltzmann equation, it is necessary to have a link between time and temperature, which is given under the assumption of adiabaticity by

$$\frac{ds_{\rm rad}}{dt} = -3Hs_{\rm rad}\,, \tag{2.9}$$

where the radiation entropy density is given by

$$s(T) = h_{\rm eff}(T)\frac{2\pi^2}{45}T^3\,, \tag{2.10}$$

with $h_{\rm eff}$ the effective number of entropic degrees of freedom of radiation.

To solve this set of equations, one defines the ratio of the number density of BSM particles to the radiation entropy density $Y(T) \equiv n(T)/s_{\rm rad}(T)$, and the ratio of the relic particle mass to the temperature, $x \equiv m_{\rm relic}/T$, and combines them into [43, 44]:

$$\frac{dY}{dx} = -\sqrt{\frac{\pi}{45G}}\frac{g_*^{1/2}m_{\rm relic}}{x^2}\langle\sigma_{\rm eff}v\rangle(Y^2 - Y_{\rm eq}^2)\,, \tag{2.11}$$

with

$$g_*^{1/2} = \frac{h_{\rm eff}}{\sqrt{g_{\rm eff}}}\left(1 + \frac{T}{3h_{\rm eff}}\frac{dh_{\rm eff}}{dT}\right)\,. \tag{2.12}$$

The freeze-out temperature T_f is the temperature at which the relic particle leaves the initial thermal equilibrium, which is expected to happen at $\sim m_{\rm relic}/10 \sim 10 - 100\,{\rm GeV}$ in many BSM WIMP scenarios.

Solving the equations down to the present temperature T_0, we find that Y approaches a constant asymptotic value and the relic density so obtained is [43, 44]:

$$\Omega_{\rm relic}h^2 = \frac{m_{\rm relic}s(T_0)Y(T_0)h^2}{\rho_c^0} \approx 2.755\times10^8\frac{m_{\rm relic}}{1\,{\rm GeV}}Y(T_0)\,, \tag{2.13}$$

where ρ_c^0 is the critical density of the Universe, given by

$$H_0^2 = \frac{8\pi G}{3}\rho_c^0\,, \tag{2.14}$$

and H_0 is the Hubble constant. The relic density can then be compared to the measurements of the dark matter density by the Planck Collaboration [1] to set constraints on the BSM scenarios.

In the following, we use `SuperIso Relic v4.0` [45–47] to compute the relic density. Since it was shown that the theoretical uncertainties due to the cross section calculation at tree level and to the uncertainties in the QCD equation of state are of the order of a tenth [36, 37, 41, 42, 48, 49], we add a 10% theoretical error to the Planck measurements and obtain the following 95% C.L. interval:

$$0.095 < \Omega h^2 < 0.1428\,. \tag{2.15}$$

JHEP10(2018)132

3 Cosmological scenarios

The standard relic density calculation can be modified by the presence of scalar fields in the early Universe, which can affect the expansion rate by adding a new energy density, generate non-thermal relic particles, or inject entropy and affect the relation between time and temperature. In the following, we consider the case of a decaying pressureless scalar field and of quintessence as realistic examples of cosmological models affecting the early Universe. Since the freeze-out occurs at $\sim 10-100\,\mathrm{GeV}$, a large deviation from the standard model of cosmology at this temperature could modify strongly the results, without having other consequences for the observable Universe. The strongest constraints that can be set on such cosmological scenarios are those from BBN. In the following, we compute BBN constraints for the scenarios of interest using `AlterBBN v2.0` [50, 51] and the conservative limits on the abundances of the elements given in [52].

3.1 Decaying primordial scalar field

We consider a pressureless scalar field ϕ of mass m_ϕ that decays into radiation with a width Γ_ϕ, and into BSM particles with a branching ratio b [34, 35]. The evolution in time of the scalar field density ρ_ϕ and the WIMP density $n = \rho_\chi/m_\chi$ can be determined from the following equations:

$$\frac{d\rho_\phi}{dt} = -3H\rho_\phi - \Gamma_\phi\rho_\phi\,, \tag{3.1}$$

$$\frac{dn}{dt} = -3Hn - \langle\sigma_{\rm eff}v\rangle\left(n^2 - n_{eq}^2\right) + \frac{b}{m_\phi}\Gamma_\phi\rho_\phi\,, \tag{3.2}$$

where $\langle\sigma_{\rm eff}v\rangle$ is the thermally-averaged WIMP annihilation cross section, n_{eq} is the WIMP equilibrium density, and H is the Hubble parameter, which depends on the total energy density in the Universe:

$$H^2 = \frac{8\pi}{3M_p^2}\left(\rho_\phi + \rho_{\rm rad} + \rho_\chi\right)\,. \tag{3.3}$$

We assume that the thermalisation of the decay products of the scalar field occurs instantaneously.[1] In order to obtain a relation between the time and the temperature, one may use the following equation for the evolution of the radiation entropy density [55]:

$$\frac{ds_{\rm rad}}{dt} = -3Hs_{\rm rad} + \frac{\Gamma_\phi\rho_\phi}{T} = -3H\left(1 - \widetilde{\Sigma}^*\right)s_{\rm rad}\,, \tag{3.4}$$

with

$$\widetilde{\Sigma}^* \equiv \frac{\Gamma_\phi\rho_\phi}{3HTs_{\rm rad}}\,. \tag{3.5}$$

The energy and entropy densities of radiation can be determined from the temperature according to:

$$\begin{cases} \rho_{\rm rad} = \dfrac{\pi^2}{30}g_{\rm eff}(T)T^4\,, \\ s_{\rm rad} = \dfrac{2\pi^2}{45}h_{\rm eff}(T)T^3\,, \end{cases} \tag{3.6}$$

[1] Discussions of the effect of other thermalisation assumptions can be found in [53, 54].

JHEP10(2018)132

where $g_{\rm eff}$ and $h_{\rm eff}$ are the number of degrees of freedom of radiation energy and the entropy, respectively. We use the QCD equation of state "B" of ref. [41] in our analysis.

The decay width may conveniently be expressed as a function of the reheating temperature T_{RH} [34, 35], which is the temperature at which the scalar field density starts to be significantly reduced:

$$\Gamma_\phi = \sqrt{\frac{4\pi^3 g_{\rm eff}(T_{RH})}{45}} \frac{T_{RH}^2}{M_p} \,. \tag{3.7}$$

We also define $\tilde{\rho}_\phi \equiv \rho_\phi/\rho_{\rm rad}$ and the initial condition $\kappa_\phi \equiv \rho_\phi(T_{\rm init})/\rho_\gamma(T_{\rm init})$.

In the following we assume that the period of interest for the relic density occurs when the radiation entropy density decreases with time, which corresponds to $\widetilde{\Sigma}^* < 1$. This imposes a maximal temperature $T_{\rm max}$ for the validity of the following discussion, which corresponds to the temperature at which $\widetilde{\Sigma}^* = 1$. The above equations can be re-written as derivatives of $Y_\phi = \rho_\phi/s_{\rm rad}$ and $Y = n/s_{\rm rad}$:

$$\frac{dY_\phi}{dx} = -\frac{\alpha_0}{x}\frac{\widetilde{\Sigma}^*}{1-\widetilde{\Sigma}^*}\left(Y_\phi + \frac{m_\chi}{x}\right) \,, \tag{3.8}$$

$$\frac{dY}{dx} = -\frac{\alpha_0}{x}\frac{s_{\rm rad}}{1-\widetilde{\Sigma}^*}\frac{1}{3H}\langle\sigma_{\rm eff} v\rangle\left(Y^2 - Y_{\rm eq}^2\right) - \frac{\alpha_0}{x}\frac{\widetilde{\Sigma}^*}{1-\widetilde{\Sigma}^*}\left(Y - \frac{b}{m_\phi}\frac{m_\chi}{x}\right) \,, \tag{3.9}$$

with

$$\alpha_0 = \frac{3 g_*^{1/2} g_{\rm eff}^{1/2}}{h_{\rm eff}} \approx 3 \,, \tag{3.10}$$

where $x = m_\chi/T$.

Eqs. (3.8) and (3.9) are controlled by the parameter $\widetilde{\Sigma}^*$ defined in eq. (3.5). In order to understand its role, we consider the entropy time-derivative equation (3.4) in the case where $\widetilde{\Sigma}^*$ is constant. If $T \propto t^\alpha$ and the scale factor $a \propto t^\beta$, then $H = \beta t^{-1}$ and we obtain:

$$3\alpha = -3\beta(1-\widetilde{\Sigma}^*) \,. \tag{3.11}$$

Thus, $\beta = -\alpha/(1-\widetilde{\Sigma}^*)$ and $a \propto t^{-\alpha/(1-\widetilde{\Sigma}^*)} \propto T^{-1/(1-\widetilde{\Sigma}^*)}$. After freeze-out, the WIMP density verifies $\rho_\chi \propto a^{-3}$, so $\rho_\chi \propto T^{3/(1-\widetilde{\Sigma}^*)}$. The WIMP density will therefore be diluted very fast as $\widetilde{\Sigma}^* \to 1$. In fact, one can derive a maximum value for $\widetilde{\Sigma}^*$ where $d\log(\widetilde{\Sigma}^*)/d\log(x) = 0$. In the limit $\rho_\phi \gg \rho_{\rm rad}$, $\widetilde{\Sigma}^* \propto x^{5/2} Y_\phi^{1/2}$ according to eq. (3.7). Thus the maximum value of $\widetilde{\Sigma}^*$ is reached when $d\log(Y_\phi)/d\log(x) = -5$. Using eq. (3.8) we obtain the condition

$$-\alpha_0 \frac{\widetilde{\Sigma}^*_{\rm MAX}}{1-\widetilde{\Sigma}^*_{\rm MAX}}\left(1 + \frac{T}{Y_\phi}\right) = \frac{d\log(Y_\phi)}{d\log(x)} = -5 \,, \tag{3.12}$$

from which it follows that

$$\frac{\widetilde{\Sigma}^*_{\rm MAX}}{1-\widetilde{\Sigma}^*_{\rm MAX}} = \frac{5}{\alpha_0}\frac{1}{1+\frac{T}{Y_\phi}} < \frac{5}{\alpha_0} \lesssim 1.66 \,, \tag{3.13}$$

JHEP10(2018)132

which leads to

$$\widetilde{\Sigma}^* < \frac{5}{\alpha_0}\frac{1}{1+\frac{5}{\alpha_0}} \approx 0.625\,. \tag{3.14}$$

This prevents any singularities in the term $\widetilde{\Sigma}^*/1-\widetilde{\Sigma}^*$, but limits the strength of the dilution.

We have seen that the scalar field density can decrease in two ways: either by decay, or by dilution. Thus, the presence of the scalar field may modify the WIMP relic density from that calculated in the standard model of cosmology in three different ways. First, WIMPs can be diluted in the same way as the scalar field. As this phenomenon only changes the evolution of the temperature with time, it does not affect the WIMP density at a given temperature during thermal equilibrium, since the equilibrium density is determined by the temperature alone. Secondly, if the scalar field decays into BSM particles, the WIMP density may increase. If the decay happens before freeze-out, however, the decay products will annihilate and there would be no consequence on the relic density.

Thirdly, if the scalar field density is large enough, it will change significantly the Hubble parameter and the freeze-out will occur sooner, thus increasing the density at freeze-out compared to the standard calculation. However, as we shall see, this last case corresponds also to that where dilution is important. Therefore, the only way to increase the relic density is if the scalar field decays also into BSM particles.

3.2 Quintessence

As an alternative, we also consider a quintessence field,[2] which satisfies the continuity equation:

$$\frac{d\rho_\phi}{dt} = 3H(\rho_\phi + P_\phi)\,, \tag{3.15}$$

where the pressure and the energy density of the scalar field are $P_\phi = \dot{\phi}^2/2 - V(\phi)$ and $\rho_\phi = \dot{\phi}^2/2 + V(\phi)$, respectively.

We have computed the scalar field density evolution with the temperature for three different standard quintessence potentials $V(\phi)$ [16]: a double exponential [56], an inverse power law [7], and a pseudo-Nambu-Goldstone boson potential [57]. We find that the scalar field density can be well approximated for the three potentials with a power law of slope 6 at high temperatures (zone 4 of figure 1) and of slope 0 at low temperatures coinciding with the measured dark energy density (zone 1). In the case of the double exponential potential, two additional power-law changes occur: the first to a slope 0 (zone 3) and then to a slope ranging from 3 to 6 (zone 2). Hence, we consider a simplified model whose free parameters are the temperatures T_{34}, T_{23}, T_{12} at which the power-law changes occur, together with the slope in zone 2, n_2.

In this model, there is no way to reduce the relic density compared to the standard cosmological model. The only possible influence of the scalar field is on the WIMP density at freeze-out. If the scalar field density is large enough while the WIMP is in thermal equilibrium, the Hubble parameter can be enhanced compared to the standard cosmological model. This would have the effect of advancing freeze-out and thereby increasing the relic WIMP density.

[2] See, for example, [16] for a review of quintessence models.

JHEP10(2018)132

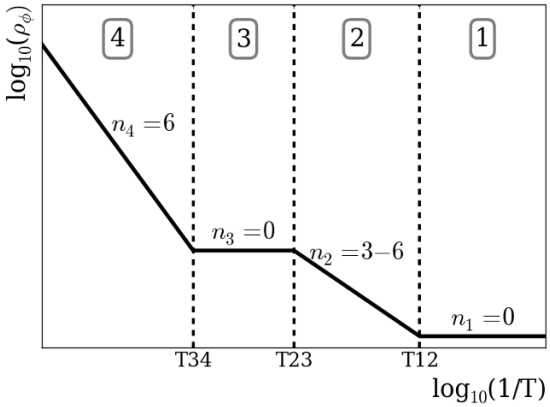

Figure 1. Evolution with temperature of the scalar field density in representative power-law models of quintessence.

4 New physics scenarios

In order to illustrate the possible implications of such cosmological scenarios, we consider variants of the minimal supersymmetric extension of the Standard Model (MSSM) with CP and R-parity conservation, which is representative of a large class of WIMP models. The lightest neutralino is a well-motivated candidate for dark matter [2], and we assume in the following that 100% of cold dark matter is composed of neutralinos. The neutralino can be bino-like, wino-like, higgsino-like or a mixed state. These candidates are weakly-interacting, and in conventional calculations bino-like neutralinos have in general a too large a relic density, apart in cases where they are associated with near-degenerate supersymmetric particles with which they can coannihilate, or if annihilations are enhanced by resonances such as heavy Higgs bosons. Winos and Higgsinos can reach a relic density close to the observed dark matter abundance via coannihilations with charginos and/or neutralinos that are nearly degenerate with the lightest neutralino. On the other hand, light winos and Higgsinos generally have too small a relic density.

In the following we first choose as specific examples one MSSM scenario which would yield overdense DM according to the standard cosmological calculation, and one that would yield underdense DM. We also consider a sample of points in the phenomenological MSSM (pMSSM) with 19 free parameters specified at a low energy scale (the pMSSM19).

4.1 Benchmark point A

We first consider a point with a relic density that would be too large (Point A) according to the standard cosmological calculation. For this we modify the parameters of the best-fit point of the pMSSM with 11 free parameters specified at a low energy scale (the pMSSM11), which was found in [58] taking into account the constraints from $\sim 36\,\mathrm{fb}^{-1}$ of LHC data at 13 TeV, including those from direct searches for supersymmetric (SUSY) particles at the LHC, measurements of the Higgs boson mass and signal strengths, LHC searches for the heavier MSSM Higgs bosons, precision electroweak observables, the measurement of

JHEP10(2018)132

M_1	M_2	M_3	μ	M_{A^0}	$\tan\beta$
-391	1240	-1714	-5739	4221	18.8

$M_{\tilde{q}_{1,2}}$	$M_{\tilde{q}_3}$	$M_{\tilde{l}_{1,2}}$	$M_{\tilde{l}_3}$	A_0
1996	4058	400	1365	5372

Table 1. The pMSSM11 parameter values (in GeV) of Point A.

M_0	M_{12}	$\tan\beta$	A_0	sign(μ)
10931	3872	52.9	9188	+1

Table 2. The CMSSM parameter values (in GeV when applicable) of Point B.

$(g-2)_\mu$ [59], and flavour physics constraints from B- and K-physics observables. In addition, the constraints from the direct dark matter detection experiments PICO60 [60], XENON1T [61] and PandaX-II [62] were taken into account, together with the previous accelerator and astrophysical measurements. The cosmological constraint on the cold dark matter density measured by Planck [1] was also considered. The relic density at this point is therefore close to the measured dark matter density, but it is possible to increase the relic density while respecting the other constraints. This point has a bino-like neutralino of mass 381 GeV. As commented above, binos tend to have a relic density that is too large. However, thanks to the small mass splittings with the sleptons of the first and second generations, the relic density of this points is very close to the measured dark matter density. In order to obtain a larger relic density, we increase the mass parameter $M_{\tilde{l}_{1,2}}$ of the sleptons of first and second generation, taking $M_{\tilde{l}_{1,2}} = 400\,\text{GeV}$. The mass of the lightest neutralino is 381 GeV and the next-to-lightest supersymmetric particles are the right-handed selectron and smuon of mass 423 GeV. The mass splitting is large enough so that the impact of the co-annihilations is limited. We obtain a relic density $\Omega h^2 = 1.27$ according to the standard cosmological calculation, and a freeze-out temperature $T_{\text{fo}} \approx 16\,\text{GeV}$. The parameters of Point A are given in table 1 and the spectrum is generated with `SOFTSUSY` [63].

4.2 Benchmark point B

In this case we modify the best-fit point in the constrained MSSM (CMSSM) found in [58]. This point has a higgsino-like neutralino and a relic density close to the dark matter density measured by Planck. We decrease M_{12} to 3872 GeV in order to get a lower value of the relic density: $\Omega h^2 = 5.907 \times 10^{-3}$ and use `SOFTSUSY` [63] to calculate the spectrum. The parameters of point B are given in table 2.

4.3 Sample of pMSSM19 points

We consider in addition a sample of points in the pMSSM19 generated using `SOFTSUSY` [63] with a flat random sampling over the ranges given in table 3 for the 19 parameters. After checking the theoretical validity of each point, we require it to have a light Higgs boson with mass between 122 and 128 GeV. We also require the lightest neutralino to be the

JHEP10(2018)132

Parameter	Range (in GeV)
M_A	[50, 2000]
M_1	[-3000, 3000]
M_2	[-3000, 3000]
M_3	[50, 3000]
$A_d = A_s = A_b$	[-10000, 10000]
$A_u = A_c = A_t$	[-10000, 10000]
$A_e = A_\mu = A_\tau$	[-10000, 10000]
μ	[-3000, 3000]
$M_{\tilde{e}_L} = M_{\tilde{\mu}_L}$	[0, 3000]
$M_{\tilde{e}_R} = M_{\tilde{\mu}_R}$	[0, 3000]
$M_{\tilde{\tau}_L}$	[0, 3000]
$M_{\tilde{\tau}_R}$	[0, 3000]
$M_{\tilde{q}_{1L}} = M_{\tilde{q}_{2L}}$	[0, 3000]
$M_{\tilde{q}_{3L}}$	[0, 3000]
$M_{\tilde{u}_R} = M_{\tilde{c}_R}$	[0, 3000]
$M_{\tilde{t}_R}$	[0, 3000]
$M_{\tilde{d}_R} = M_{\tilde{s}_R}$	[0, 3000]
$M_{\tilde{b}_R}$	[0, 3000]
$\tan\beta$	[1, 60]

Table 3. The pMSSM19 parameter ranges used in our scan.

lightest supersymmetric particle that constitutes dark matter, using the set-up presented in [64–66]. As the neutralino can be bino-like, wino-like, Higgsino-like or a mixed state, this approach allows considerable flexibility, making our analysis sufficiently general that it can indicate the possibilities also in other dark matter models.

5 Results

5.1 Decaying primordial scalar field

We consider first the cosmological scenario with a scalar field decaying into radiation and SUSY particles. We perform a scan over the reheating temperature T_{RH} and the initial scalar field density parametrised as the ratio between the scalar field density and the photon density at $T = T_{\rm init}$, $\kappa_\phi = \frac{\rho_\phi}{\rho_\gamma}(T = T_{\rm init})$, and calculate the relic density of Points A and B specified in section 4. We consider different values of the parameter $\eta = b\left(\frac{1\,\mathrm{GeV}}{m_\phi}\right)$, in order to study the effect of non-thermal production of SUSY particles on the relic density. In each case we derive constraints on the scalar field parameters for our sample of pMSSM19

JHEP10(2018)132

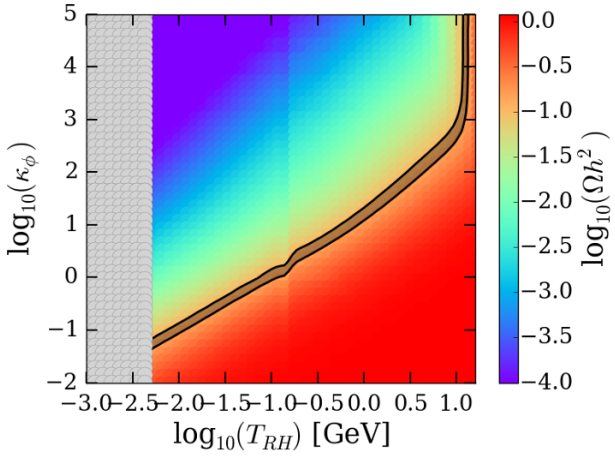

Figure 2. The relic density $\log_{10}(\Omega h^2)$ of Point A, indicated by the colour code in the legend, as a function of T_{RH} and κ_ϕ. Parameter sets consistent with the Planck constraints lie along the darker shaded strip. The grey zone at small T_{RH} is excluded by BBN constraints.

points so as to investigate the influence of the neutralino properties on the limits derived from the relic DM density.

We start integrating the Boltzmann equations at a temperature $T_{\rm init} = 40\,\text{GeV}$ for point A and $T_{\rm init} = 20\,\text{GeV}$ for point B. For our sample of pMSSM19 points, we use $T_{\rm init} = 1.5 \times T_{\rm fo}$, where $T_{\rm fo}$ is the freeze-out temperature in the standard cosmological model. These choices were made in order to reduce the computation time while starting the calculation sufficiently long before freeze-out and the decay of the scalar field.

5.1.1 Point with a large relic density

We first investigate the case where the neutralino has a relic density that is too large in the standard cosmological model, illustrated by Point A. The results of the scan over the reheating temperature T_{RH} and the initial scalar field density κ_ϕ are shown in figure 2, assuming that the scalar field does not decay into SUSY particles ($\eta = 0$). We can distinguish two zones in this figure: a zone at large initial scalar field density and small reheating temperature, where the relic density is strongly reduced, and the complementary zone where the presence of the scalar field does not modify the relic density. On the one hand, the dependence on κ_ϕ of the dilution is rather clear: the larger κ_ϕ is, the larger $\widetilde{\Sigma}^*$ is initially, and the dilution is stronger. On the other hand, the value of the reheating temperature affects more the duration of the dilution than its strength. As illustrated in figure 3, when T_{RH} is small, $\widetilde{\Sigma}^*$ can remain at its maximum during a large range of temperatures before its decrease due to the decay of the scalar field. The neutralino and scalar field densities decrease during this period with a slope -5, as expected when $\widetilde{\Sigma}^*$ is at its maximum. For a large value of T_{RH}, however, the fields are diluted over a smaller range of temperatures and the total decrease is reduced.

Points respecting the Planck constraints, which we will refer to as *accepted points*, lie along a thin line in the $\log_{10}(\kappa_\phi)/\log_{10}(T_{RH})$ plane. They follow a line of slope ~ 1 at small

JHEP10(2018)132

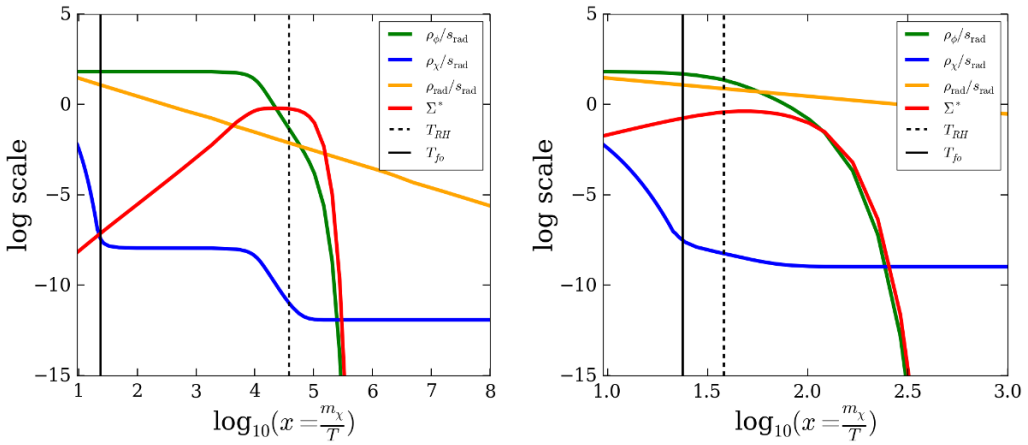

(a) $T_{RH} = 0.01\,\text{GeV}$, $\kappa_\phi = 100$, $T_{\rm init} = 40\,\text{GeV}$ **(b)** $T_{RH} = 10\,\text{GeV}$, $\kappa_\phi = 100$, $T_{\rm init} = 40\,\text{GeV}$

Figure 3. The evolution of the scalar field, neutralino and radiation densities normalised to the radiation entropy density, and of the injection of entropy $\widetilde{\Sigma}^*$, as a function of $x = m_\chi/T$.

T_{RH} that changes slightly at $T_{RH} \sim 150\,\text{MeV}$ to a slope 1.5. This transition is the result of the quark/hadronic phase transition, which lowers the number of radiation degrees of freedom. In particular, below $T \sim 150\,\text{MeV}$, pions become non-relativistic and no longer contribute to the radiation density. This feature is independent of the WIMP and scalar field properties, and is present in all the following results.

The line of accepted points becomes vertical at $T_{RH} \sim T_{\rm fo}$, which is to be expected when the scalar field decays completely during neutralino thermal equilibrium, as there is no possible modification of the relic density. Thus, we can derive a maximum value of the reheating temperature $T_{RH} \lesssim T_{\rm fo}$. One can also note that if $T_{RH} < T_{RH}^{\rm BBN\,lim} \sim 6\,\text{MeV}$, the scalar field density is too large during BBN, and the model is therefore excluded. This constraint is very general, as it is also independent of the WIMP properties, and thus applicable to any WIMP model. This limit gives us a lower bound for the reheating temperature, as well as a minimum value for the initial scalar field density κ_ϕ using $T_{RH} = T_{RH}^{\rm BBN\,lim}$. For Point A, we can deduce $\kappa_\phi \gtrsim 0.1$, but this minimum value will depend on the nature of the WIMP.

No enhancement of the relic density is possible when $\eta = 0$. At small T_{RH} and large κ_ϕ, where the scalar field density could have increased the freeze-out temperature via its relation with the Hubble parameter, and thereby increased the relic density, the densities are in fact already significantly reduced by dilution. Therefore, in order to increase the relic density, it is necessary to consider non-thermal production of the WIMP, i.e., $\eta > 0$. In the case of Point A, the region of interest will be at small T_{RH} and large κ_ϕ, where the relic density is strongly reduced by dilution. The scalar field decay into SUSY particles provides an additional contribution to the relic density, and the DM density measured by Planck may be reached with the appropriate value of η. We test four different values of η in figure 4, and notice that the larger η is, the more the line of accepted points is shifted towards small T_{RH}.

JHEP10(2018)132

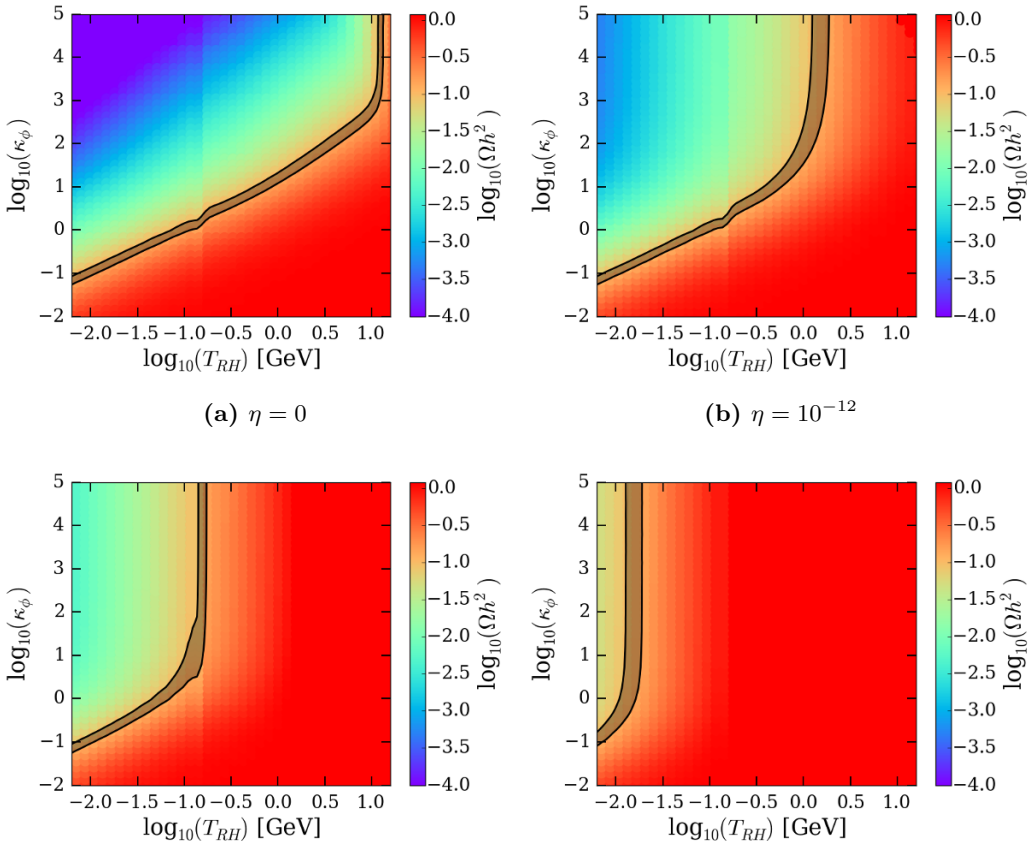

(a) $\eta = 0$ **(b)** $\eta = 10^{-12}$

(c) $\eta = 10^{-11}$ **(d)** $\eta = 10^{-10}$

Figure 4. The effect of varying η on $\log_{10}(\Omega h^2)$ for Point A, indicated by the colour code in the legend.

We observe in figure 5 that in the region of interest the relic density increases linearly with η and T_{RH}, which explains the observed feature. Similarly to what happens with the dilution, the parameter η impacts the strength of the non-thermal production of neutralinos, while T_{RH} impacts the time between the freeze-out and the scalar field decay, during which the relic density can benefit from this new contribution.

In the limit of large κ_ϕ and small T_{RH}, we find that the evolution of the relic density with respect to η and T_{RH} can be approximated by:

$$\Omega h^2 \approx \eta \left(\alpha \, T_{RH} + \beta\right), \tag{5.1}$$

where α and β are numerical factors that depend, *a priori*, on the WIMP properties. When η goes to zero, the relic density vanishes, which is expected since, in this region of the parameter space, the dilution due to the entropy injection is dominant in absence of non-thermal production. One can also note that the effects of the dilution and of the non-thermal production equilibrate in such a way that the above expression does not depend on κ_ϕ. For Point A, we find that $\alpha \approx 7.68 \times 10^{10}$ GeV^{-1} and $\beta \approx 2.62 \times 10^{7}$. This

JHEP10(2018)132

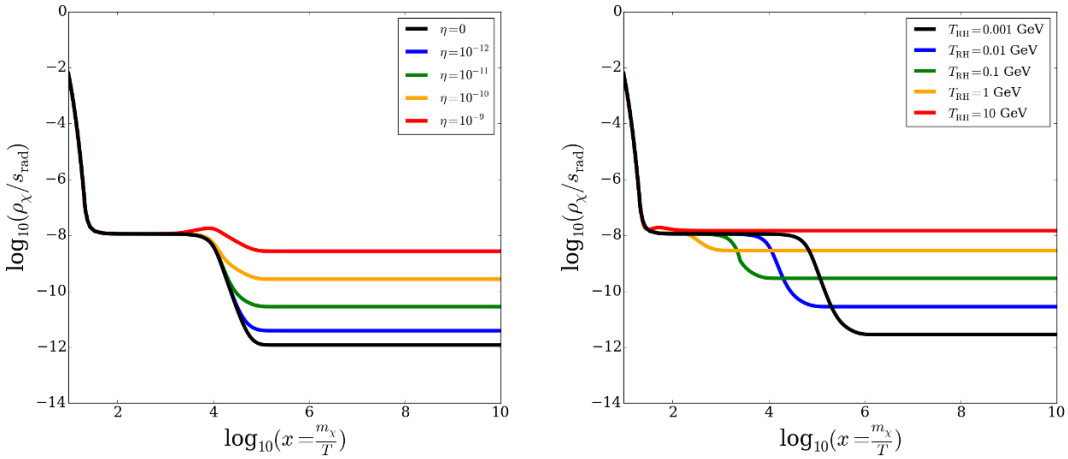

(a) **(b)**

Figure 5. The variation of the relic density normalised to the radiation entropy density as a function of the temperature, for $T_{\rm init} = 40\,\text{GeV}$ and $\kappa_\phi = 100$, when (a) varying the value of η with fixed $T_{RH} = 0.01\,\text{GeV}$, and (b) varying the value of T_{RH} with fixed $\eta = 10^{-11}$.

parametrisation enables us to find the value of η required to get the correct relic density for a given reheating temperature. On the other hand, a maximum value of η can be calculated by considering the reheating temperature where the BBN constraints start excluding the model ($T_{RH}^{\rm lim} \approx 6 \times 10^{-3}\,\text{GeV}$):

$$\eta_{\rm Max} = \frac{\Omega h^2{}^{\rm upper\,lim}_{\rm DM}}{\alpha T_{RH}^{\rm lim} + \beta}\ . \tag{5.2}$$

For our benchmark point, we calculate $\eta_{\rm Max} \approx 2.93 \times 10^{-10}$. Thus, in this scenario the branching ratio into SUSY particles must be very small, which can be traced back to our choice of a scalar field with a substantial initial density. We note also that the variation in η does not modify the constraints on κ_ϕ and T_{RH} that we derived in the case $\eta = 0$. Strong constraints on the scalar field parameters can therefore be derived, namely $6\,\text{MeV} \lesssim T_{RH} \lesssim T_{\rm fo}$, $\kappa_\phi \gtrsim 0.1$ and $\eta \lesssim 2.93 \times 10^{-10}$.

5.1.2 Point with a small relic density

As discussed previously, no enhancement of the relic density is possible when only entropy injection is considered. Therefore, one needs to allow the scalar field to decay into BSM particles. We show in figure 6 the result of scans over T_{RH} and κ_ϕ for Point B with four different values of η. In each scenario, the region of accepted points forms a U shape in the κ_ϕ /T_{RH} plane. The vertical right limit corresponds to $T_{RH} \sim T_{\rm fo}$, and does not move significantly as η increases. The vertical left limit, however, is shifted to the left along the T_{RH} axis and the horizontal limit is shifted downwards towards lower values of κ_ϕ. The constraints on T_{RH} that we deduced for point A hold also in this case: $T_{RH}^{\rm BBN\,lim} \lesssim T_{RH} \lesssim T_{\rm fo}$. However, it is difficult to find limits on κ_ϕ and η as stringent as the ones we found for point A.

JHEP10(2018)132

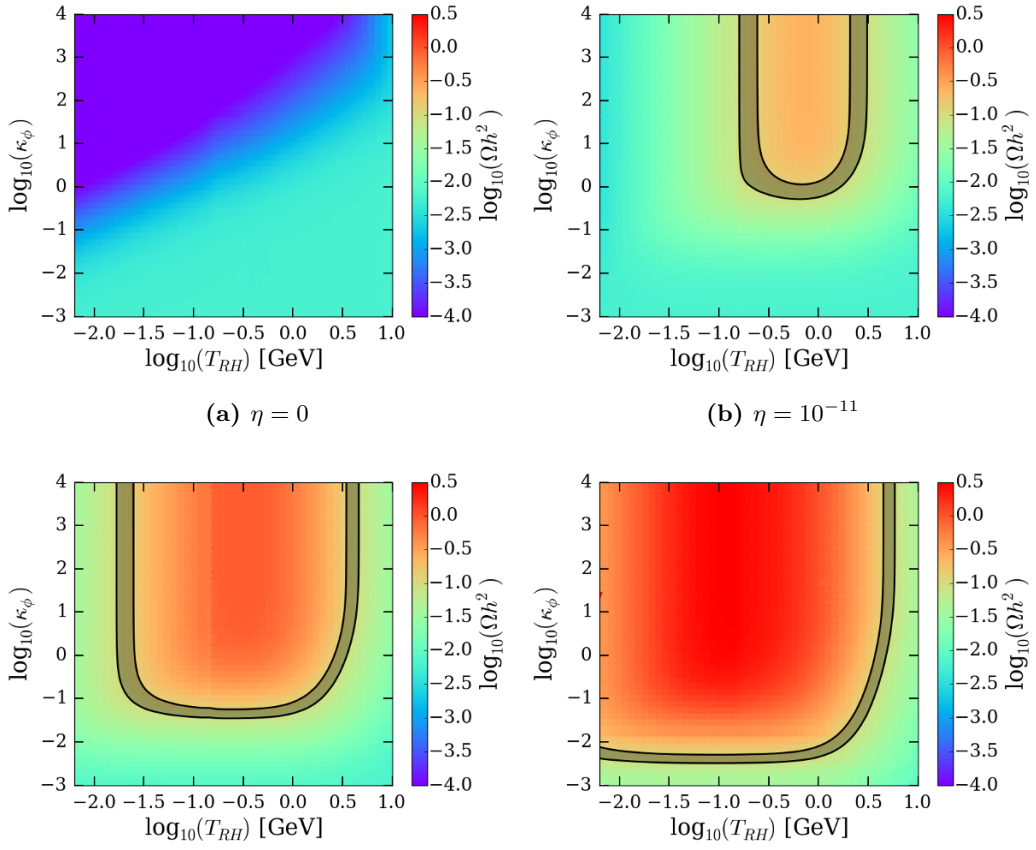

(a) $\eta = 0$ **(b)** $\eta = 10^{-11}$

(c) $\eta = 10^{-10}$ **(d)** $\eta = 10^{-9}$

Figure 6. The effect of varying η on $\log_{10}(\Omega h^2)$ for Point B, indicated by the colour code in the legend.

The largest effect is in the case where the scalar field decays entirely into BSM particles and not into radiation. Thus, if a decay produces two SUSY particles, for example, $b = 2$ and $m_\phi > 2m_\chi$, so $\eta < 1/m_\chi$. In such a case, all the SUSY particles produced by the scalar field decay, starting from the neutralino freeze-out, constitute an overall contribution to the relic density that has to be added to the value of the relic density in the standard model, i.e., $Y = Y_{\text{stand}} + Y_\phi^{\text{T=T}_{\text{fo}}}/m_\chi$. Therefore, one has a constraint on the scalar field density at freeze-out.

5.1.3 pMSSM19 sample

In the following, we study how the constraints on the scalar field depend on the WIMP properties disregarding the case of a relic density that is too small, as the constraints deduced in this case already showed an explicit dependence on the freeze-out temperature and the relic density at freeze-out.

We focus on the points in our pMSSM19 sample that have a relic density that is too large in the standard cosmological model, which leaves us almost exclusively with bino-

JHEP10(2018)132

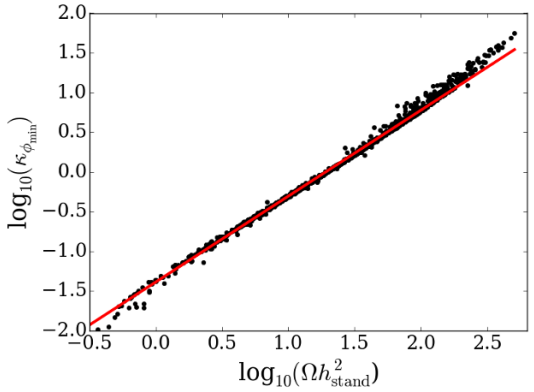

Figure 7. The values of κ_ϕ required to reduce the relic density to the measured DM density with $T_{RH} = T_{RH}^{\rm BBN\,lim}$ and $T_{\rm init} = 40\,{\rm GeV}$ as a function of the relic density calculated in the standard model of cosmology. The calculations were done for the sample of points in the pMSSM19 characterised in table 3.

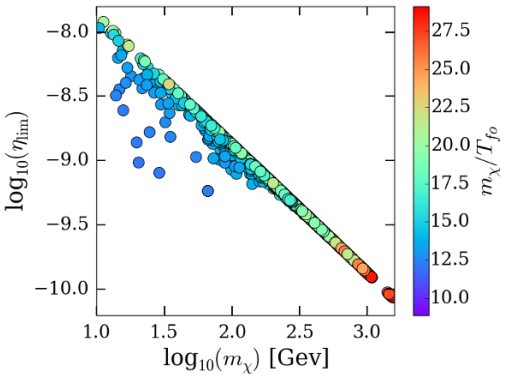

Figure 8. The maximum value of the parameter η for the pMSSM19 sample of points as a function of the neutralino mass. The values of $m_\chi/T_{\rm fo}$ are colour-coded as indicated in the legend.

like neutralinos. We calculated the values of κ_ϕ that give the correct relic density at $T_{RH} = T_{RH}^{\rm BBN\,lim}$, as shown in figure 7, and find a very good correlation between the relic density calculated in the standard model and $\kappa_{\phi_{\min}}$.

The points in figure 7 follow a line of slope ~ 1. Thus, the minimum value of the initial scalar field density increases with the value of the relic density in the standard model. This can be understood because the larger the relic density at freeze-out is, the stronger must be the dilution for a given reheating temperature. The small scatter of the points at low relic density is due to numerical uncertainties alone, but we note a departure from this line at large $\Omega h^2_{\rm stand}$, when $\kappa_{\phi_{\min}} \gtrsim 1$. With a scalar field density of this order of magnitude, there is also a modification of the Hubble parameter, which advances freeze-out. This mechanism tends to increase the relic density, while the entropy injection decreases it. Overall, the dilution has a stronger effect, but a larger scalar field density is required to decrease the relic density down to the measured DM density.

Next, we calculate the maximum value of η and find a clear dependence on the WIMP mass, as seen in figure 8. Indeed, the scalar field produces a fraction b of SUSY particles, which contributes as $m_\chi \times b$ to the WIMP mass density. Therefore, the larger m_χ is, the more the relic density will be increased for a given value of η, and the smaller will be the maximum value of η. At first approximation, the maximum value of η is inversely proportional to the WIMP mass. However, another mechanism is at play: for the same neutralino mass, the larger $T_{\rm fo}$ is, the larger the neutralino density at the freeze-out temperature is, and thus the smaller η must be in order to reach the correct relic density. As $T_{\rm fo_{stand}} \approx m_\chi/20$, we can express a linear relation between $\eta_{\rm lim}$ and m_χ. However, as shown in figure 8, when $T_{\rm fo}$ departs from this approximation towards larger values, the second mechanism becomes more important, and we see a departure from the linear relation be-

JHEP10(2018)132

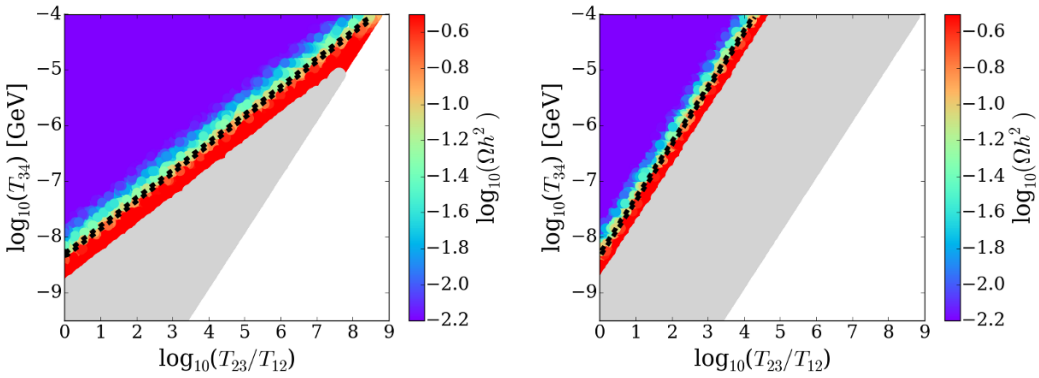

(a) $n_2 = 3$ **(b)** $n_2 = 6$

Figure 9. The value of $\log_{10}(\Omega h^2)$, colour-coded as indicated in the legend, in the T_{34}, T_{23}/T_{12} parameter plane of the quintessence model. The accepted parameter sets lie between the two dashed lines, the grey region is excluded by BBN and the white one is not accessible in this model.

tween m_χ and $\eta_{\rm lim}$. This happens for neutralino masses smaller than $\sim 100\,\text{GeV}$ in our sample of points. In any case, η must be very small, of the order of $\sim 10^{-10}$–10^{-9}.

5.2 Quintessence

We now turn to the study of the quintessence model. This scenario only has the power to increase the relic density by advancing freeze-out. Therefore, we disregard the case of a standard relic density that is too large.

5.2.1 Point with a small relic density

We have scanned over the three temperature parameters such that $T_0 < T_{12} < T_{23} < T_{34}$ with $T_0 = 2 \times 10^{-13}\,\text{GeV}$, the temperature of the CMB at present time. We performed the scans for the two extreme values of the slope in zone 2 of figure 1, namely $n_2 = 3$ and $n_2 = 6$. We have calculated the relic density of our benchmark CMSSM point for each set of quintessence parameters, and show the results in figure 9.

The relevant parameters are T_{34} and the ratio T_{23}/T_{12}. The smaller T_{34} is, and the greater T_{23}/T_{12} is, the larger is the relic density. This can easily be understood as the larger the scalar field density is around freeze-out, the larger will be the increase of the relic density, and a small value of T_{34} and a large difference between T_{12} and T_{23} helps in obtaining a large scalar field density at large temperatures. In the case $n_2 = 3$, the accepted parameter sets follow a line of slope ~ 0.5, and we find a limit at $T_{23}/T_{12} \sim 6 \times 10^8$ and $T_{34} \sim 10^{-4}\,\text{GeV}$, where the line reaches the limiting case $T_{34} = T_{23}$. A minimum value of T_{34} can be found when $T_{12} = T_{23}$, where we find $T_{34} \gtrsim 2 \times 10^{-9}\,\text{GeV}$. In the case where $n_2 = 6$, the same minimal value can be found. However, the accepted parameter sets follow a line of slope 1, parallel to the limit $T_{23} = T_{34}$. There are, therefore, no maximum values for the temperature parameters.

JHEP10(2018)132

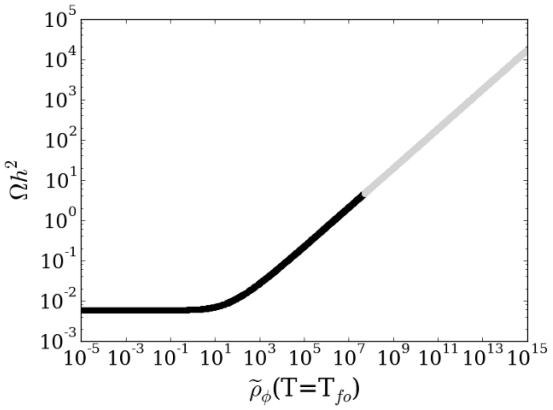

Figure 10. The increase in the relic density for Point B as a function of the ratio of the scalar density and the radiation density at 1 MeV. The grey region is excluded by BBN.

In both cases, we note also that the accepted parameter sets are very close to the limit imposed by BBN, which mainly depends on the density of the scalar field at a temperature $T \sim 1\,\mathrm{MeV}$.

When T_{34} is smaller than 1 MeV, which must be the case for values of n_2 close to 3, it is possible to find simpler constraints on the scalar field properties. In this case, freeze out and BBN both occur during phase 4 of the scalar field evolution in the model. The scalar field density can thus be specified simply by its value at freeze-out, and determined at other temperatures according to the slope $n_4 = 6$. We can therefore disregard what happens in phases 1, 2 and 3. We show in figure 10 the evolution of the relic density for Point B with the ratio of the scalar field density to the radiation density at freeze-out, $\widetilde{\rho}_\phi = \frac{\rho_\phi}{\rho_{\mathrm{rad}}}(T = T_{\mathrm{fo}})$ when we consider only phase 4 of the model.

The scalar field starts having an effect on the relic density when its density is comparable to the radiation density at freeze-out. The Hubble parameter is thus significantly modified and freeze-out is advanced. The relic density then increases with a slope ~ 0.48. In addition, we note that points are excluded by BBN if $\frac{\rho_\phi}{\rho_{\mathrm{rad}}}(\mathrm{T}{=}T_{\mathrm{fo}}) \gtrsim 10^8$, which corresponds to $\frac{\rho_\phi}{\rho_{\mathrm{rad}}}(1\,\mathrm{MeV}) \gtrsim 1$.

5.2.2 pMSSM19 sample

In addition, we have calculated the value of $\widetilde{\rho}_\phi(T = T_{\mathrm{fo}})$ required to obtain the correct relic density in our sample of pMSSM19 points. The result is shown in figure 11, which shows the dependence of $\widetilde{\rho}_\phi(T = T_{\mathrm{fo}})$ on the standard relic density.

In a first approximation, $\widetilde{\rho}_\phi(T = T_{\mathrm{fo}})$ scales as a power of the standard relic density, with an exponent ~ -2. The smaller the standard relic density is, the larger the scalar field density must be around freeze-out in order to increase the relic density up to the DM density. The exponent -2 can be understood from a simple calculation. Freeze-out occurs when the annihilation rate equals the expansion rate, in the standard cosmological model:

$$n_{\mathrm{eq}}(T_{\mathrm{fo}}^{\mathrm{stand}})\langle\sigma_{\mathrm{eff}}v\rangle_{T_{\mathrm{fo}_{\mathrm{stand}}}} \sim H \sim H_0\rho_{\mathrm{rad}}^{1/2}(T = T_{\mathrm{fo}_{\mathrm{stand}}})\,, \tag{5.3}$$

JHEP10(2018)132

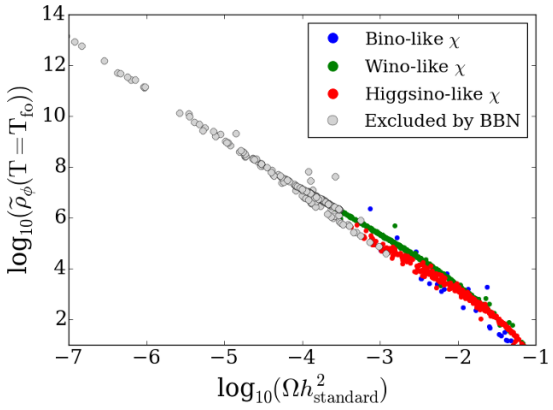

Figure 11. The value of the scalar field density at freeze-out that is required to increase the relic density up to the observed DM density for our sample of pMSSM19 points. The neutralino mass is shown in colour and parameter sets excluded by BBN are shown in grey.

with $H_0 = \sqrt{8\pi/3M_p^2}$. The comoving neutralino density $Y_{\rm stand}$ can then be expressed as:

$$Y_{\rm stand} = \frac{n_{\rm eq}(T_{\rm fo_{stand}})}{s_{\rm rad}(T_{\rm fo_{stand}})}\,, \tag{5.4}$$

which can be re-expressed using eq. (5.3) as

$$Y_{\rm stand} = \frac{H_0 \rho_{\rm rad}^{1/2}(T_{\rm fo_{stand}})}{\langle\sigma_{\rm eff} v\rangle_{T_{\rm fo_{stand}}} s_{\rm rad}(T_{\rm fo_{stand}})}\,. \tag{5.5}$$

When the scalar field density is very large in the quintessence model, compared to the radiation density, we obtain similar equations:

$$n_{\rm eq}(T_{\rm fo})\langle\sigma_{\rm eff} v\rangle_{T=T_{\rm fo}} \sim H \sim H_0 \rho_\phi^{1/2}(T=T_{\rm fo}) = H_0 \rho_\phi^{1/2}(T=T_{\rm fo_{stand}}) \times \left(\frac{T_{\rm fo}}{T_{\rm fo_{stand}}}\right)^3\,, \tag{5.6}$$

and

$$Y = \frac{n_{\rm eq}(T_{\rm fo})}{s_{\rm rad}(T_{\rm fo})}\,, \tag{5.7}$$

where we have used in eq. (5.6) the fact that the scalar field density evolves as T^{n_4} with $n_4 = 6$. The relic comoving density Y in this scenario can then be re-written using eq. (5.6) as:

$$Y = \frac{H_0 \rho_\phi^{1/2}(T=T_{\rm fo_{stand}}) \times \left(\frac{T_{\rm fo}}{T_{\rm fo_{stand}}}\right)^3}{\langle\sigma_{\rm eff} v\rangle_{T_{\rm fo}} s_{\rm rad}(T_{\rm fo})} = \frac{H_0 \rho_\phi^{1/2}(T=T_{\rm fo_{stand}})}{\langle\sigma_{\rm eff} v\rangle_{T_{\rm fo}} s_{\rm rad}(T_{\rm fo_{stand}})}\,. \tag{5.8}$$

Finally, we can combine eqs. (5.8) and (5.5) to obtain:

$$Y = Y_{\rm stand} \frac{\langle\sigma_{\rm eff} v\rangle_{T_{\rm fo_{stand}}}}{\langle\sigma_{\rm eff} v\rangle_{T_{\rm fo}}} \frac{\rho_\phi^{1/2}(T=T_{\rm fo_{stand}})}{\rho_{\rm rad}^{1/2}}\,. \tag{5.9}$$

JHEP10(2018)132

This gives us the ratio between the scalar field density and the radiation density at the standard freeze-out temperature that is required to increase the relic density to the measured dark matter density:

$$\begin{aligned}\widetilde{\rho}_\phi(T_{\mathrm{fo}_{\mathrm{stand}}}) &= \left(\frac{Y}{Y_{\mathrm{stand}}}\right)^2 \times \left(\frac{\langle\sigma_{\mathrm{eff}}v\rangle_{T_{\mathrm{fo}}}}{\langle\sigma_{\mathrm{eff}}v\rangle_{T_{\mathrm{fo}_{\mathrm{stand}}}}}\right)^2 \\ &= \left(\frac{\Omega h^2_{DM}}{\Omega h^2_{\mathrm{stand}}}\right)^2 \times \left(\frac{Y(T=T_{\mathrm{fo}})/Y(T=\text{present})}{Y_{\mathrm{stand}}(T=T_{\mathrm{fo}_{\mathrm{stand}}})/Y_{\mathrm{stand}}(T=\text{present})}\right)^2 \times \left(\frac{\langle\sigma_{\mathrm{eff}}v\rangle_{T_{\mathrm{fo}}}}{\langle\sigma_{\mathrm{eff}}v\rangle_{T_{\mathrm{fo}_{\mathrm{stand}}}}}\right)^2 .\end{aligned} \tag{5.10}$$

We retrieve here the slope -2. We note, however, that this particular value appears only because $n_4 = 6$, and thus depends on the quintessence model. Residual annihilations occurring after freeze-out are taken into account by the factor

$$\xi = \left(\frac{Y(T=T_{\mathrm{fo}})/Y(T=\text{present})}{Y_{\mathrm{stand}}(T=T_{fo_{\mathrm{stand}}})/Y_{\mathrm{stand}}(T=\text{present})}\right)^2 ,$$

which takes a value ~ 10 in our sample of pMSSM19 points. It was indeed already noted in [40] that the residual annihilations, so-called *relentless annihilations*, can be particularly important when $H \propto T^{2+\frac{n}{2}}$, with $n \geq 2$. In the case of the quintessence model, $n = 2$, which corresponds well to this regime. The value of ξ is model-dependent, however, and we show in figure 11 that wino-like neutralinos, for instance, require a larger scalar field density than higgsino-like neutralinos.

Finally, we note that for neutralinos with a standard relic density $\lesssim 3 \times 10^{-4}$, the scalar field density is too large at 1 MeV and our scenario is ruled out by BBN.

6 Conclusions

The cosmological density of cold dark matter is now known with good accuracy, thanks to measurements by Planck and other cosmological and astrophysical observations. We have studied in this paper how this knowledge could be used to constrain possible non-standard evolution of the early Universe in specific dark matter scenarios. An optimist might assume that laboratory experiments would establish the parameters of some scenario for physics beyond the Standard Model sufficiently well for a discrepancy to be established between the cosmological measurements and model calculations in standard radiation-dominated cosmology. More conservatively, the combination of observations and model calculations could be used to constrain a combination of model parameters and early-Universe scenarios.

As examples of non-standard evolution in the early Universe before Big Bang Nucleosynthesis, we have considered scenarios in which a scalar field decays into some combination of Standard Model and other particles, and quintessence models with various classes of effective potential. Our calculations were illustrated using various supersymmetric models in which a calculation of the cold dark matter density assuming a conventional radiation-dominated early Universe would yield a density that is either larger or smaller than the observed density. The measured cold dark matter density could be used in the case of

JHEP10(2018)132

a decaying scalar field to constrain the initial density of the scalar field, the reheating temperature after it decays, and the branching ratio for its decays into particles beyond the Standard Model. In the case of a quintessence model, the cold dark matter density could be used to constrain the evolution with temperature in the early Universe of the quintessence field.

Our results exemplify the idea that measurements by laboratory experiments could be used, in the context of a specific model for physics beyond the Standard Model, to constrain aspects of the physics controlling the evolution of the early Universe that would otherwise be invisible and inaccessible. In this way, collider and other laboratory experiments could serve as powerful telescopes, using dark matter particles as a novel type of messenger particle able to provide information about the early Universe that photons and neutrinos cannot provide.

Acknowledgments

The work of JE was supported in part by the United Kingdom STFC Grant ST/P000258/1, and in part by the Estonian Research Council via a Mobilitas Pluss grant.

References

[1] Planck collaboration, P.A.R. Ade et al., *Planck 2015 results. XIII. Cosmological parameters*, *Astron. Astrophys.* **594** (2016) A13 [arXiv:1502.01589] [INSPIRE].

[2] G. Jungman, M. Kamionkowski and K. Griest, *Supersymmetric dark matter*, *Phys. Rept.* **267** (1996) 195 [hep-ph/9506380] [INSPIRE].

[3] K.A. Olive, G. Steigman and T.P. Walker, *Primordial nucleosynthesis: Theory and observations*, *Phys. Rept.* **333** (2000) 389 [astro-ph/9905320] [INSPIRE].

[4] V. Barger, J.P. Kneller, H.-S. Lee, D. Marfatia and G. Steigman, *Effective number of neutrinos and baryon asymmetry from BBN and WMAP*, *Phys. Lett.* **B 566** (2003) 8 [hep-ph/0305075] [INSPIRE].

[5] B.D. Fields, P. Molaro and S. Sarkar, *Big-Bang Nucleosynthesis*, *Chin. Phys.* **C 38** (2014) 339 [arXiv:1412.1408] [INSPIRE].

[6] C. Wetterich, *The Cosmon model for an asymptotically vanishing time dependent cosmological 'constant'*, *Astron. Astrophys.* **301** (1995) 321 [hep-th/9408025] [INSPIRE].

[7] P.G. Ferreira and M. Joyce, *Cosmology with a primordial scaling field*, *Phys. Rev.* **D 58** (1998) 023503 [astro-ph/9711102] [INSPIRE].

[8] S. Capozziello, S. Nojiri and S.D. Odintsov, *Unified phantom cosmology: Inflation, dark energy and dark matter under the same standard*, *Phys. Lett.* **B 632** (2006) 597 [hep-th/0507182] [INSPIRE].

[9] B. Ratra and P.J.E. Peebles, *Cosmological Consequences of a Rolling Homogeneous Scalar Field*, *Phys. Rev.* **D 37** (1988) 3406 [INSPIRE].

JHEP10(2018)132

[10] I. Zlatev, L.-M. Wang and P.J. Steinhardt, *Quintessence, cosmic coincidence and the cosmological constant*, *Phys. Rev. Lett.* **82** (1999) 896 [astro-ph/9807002] [INSPIRE].

[11] L. Amendola, *Coupled quintessence*, *Phys. Rev.* **D 62** (2000) 043511 [astro-ph/9908023] [INSPIRE].

[12] R.R. Caldwell, *A Phantom menace?*, *Phys. Lett.* **B 545** (2002) 23 [astro-ph/9908168] [INSPIRE].

[13] T. Chiba, T. Okabe and M. Yamaguchi, *Kinetically driven quintessence*, *Phys. Rev.* **D 62** (2000) 023511 [astro-ph/9912463] [INSPIRE].

[14] M.C. Bento, O. Bertolami and A.A. Sen, *Generalized Chaplygin gas, accelerated expansion and dark energy matter unification*, *Phys. Rev.* **D 66** (2002) 043507 [gr-qc/0202064] [INSPIRE].

[15] S. Nojiri and S.D. Odintsov, *Unifying phantom inflation with late-time acceleration: Scalar phantom-non-phantom transition model and generalized holographic dark energy*, *Gen. Rel. Grav.* **38** (2006) 1285 [hep-th/0506212] [INSPIRE].

[16] S. Tsujikawa, *Quintessence: A Review*, *Class. Quant. Grav.* **30** (2013) 214003 [arXiv:1304.1961] [INSPIRE].

[17] P.J.E. Peebles, *Fluid dark matter*, *Astrophys. J.* **534** (2000) L127 [astro-ph/0002495] [INSPIRE].

[18] N. Bilic, G.B. Tupper and R.D. Viollier, *Unification of dark matter and dark energy: The Inhomogeneous Chaplygin gas*, *Phys. Lett.* **B 535** (2002) 17 [astro-ph/0111325] [INSPIRE].

[19] A. Arbey, *Dark fluid: A Complex scalar field to unify dark energy and dark matter*, *Phys. Rev.* **D 74** (2006) 043516 [astro-ph/0601274] [INSPIRE].

[20] F.L. Bezrukov and M. Shaposhnikov, *The Standard Model Higgs boson as the inflaton*, *Phys. Lett.* **B 659** (2008) 703 [arXiv:0710.3755] [INSPIRE].

[21] F. Bezrukov, A. Magnin, M. Shaposhnikov and S. Sibiryakov, *Higgs inflation: consistency and generalisations*, *JHEP* **01** (2011) 016 [arXiv:1008.5157] [INSPIRE].

[22] M. Dine, L. Randall and S.D. Thomas, *Supersymmetry breaking in the early universe*, *Phys. Rev. Lett.* **75** (1995) 398 [hep-ph/9503303] [INSPIRE].

[23] T. Banks, M. Berkooz and P.J. Steinhardt, *The Cosmological moduli problem, supersymmetry breaking and stability in postinflationary cosmology*, *Phys. Rev.* **D 52** (1995) 705 [hep-th/9501053] [INSPIRE].

[24] T. Moroi and T. Takahashi, *Effects of cosmological moduli fields on cosmic microwave background*, *Phys. Lett.* **B 522** (2001) 215 [*Erratum ibid.* **B 539** (2002) 303] [hep-ph/0110096] [INSPIRE].

[25] S. Nakamura and M. Yamaguchi, *Gravitino production from heavy moduli decay and cosmological moduli problem revived*, *Phys. Lett.* **B 638** (2006) 389 [hep-ph/0602081] [INSPIRE].

[26] B. de Carlos, J.A. Casas, F. Quevedo and E. Roulet, *Model independent properties and cosmological implications of the dilaton and moduli sectors of* $4-D$ *strings*, *Phys. Lett.* **B 318** (1993) 447 [hep-ph/9308325] [INSPIRE].

[27] M. Gasperini and G. Veneziano, *Dilaton production in string cosmology*, *Phys. Rev.* **D 50** (1994) 2519 [gr-qc/9403031] [INSPIRE].

[28] M. Kamionkowski and M.S. Turner, *thermal relics: do we know their abundances?*, *Phys. Rev.* **D 42** (1990) 3310 [INSPIRE].

JHEP10(2018)132

[29] P. Salati, *Quintessence and the relic density of neutralinos*, *Phys. Lett.* **B 571** (2003) 121 [astro-ph/0207396] [INSPIRE].

[30] F. Rosati, *Quintessential enhancement of dark matter abundance*, *Phys. Lett.* **B 570** (2003) 5 [hep-ph/0302159] [INSPIRE].

[31] D. Comelli, M. Pietroni and A. Riotto, *Dark energy and dark matter*, *Phys. Lett.* **B 571** (2003) 115 [hep-ph/0302080] [INSPIRE].

[32] C. Pallis, *Massive particle decay and cold dark matter abundance*, *Astropart. Phys.* **21** (2004) 689 [hep-ph/0402033] [INSPIRE].

[33] C. Pallis, *Quintessential kination and cold dark matter abundance*, *JCAP* **10** (2005) 015 [hep-ph/0503080] [INSPIRE].

[34] G.B. Gelmini and P. Gondolo, *Neutralino with the right cold dark matter abundance in (almost) any supersymmetric model*, *Phys. Rev.* **D 74** (2006) 023510 [hep-ph/0602230] [INSPIRE].

[35] G. Gelmini, P. Gondolo, A. Soldatenko and C.E. Yaguna, *The Effect of a late decaying scalar on the neutralino relic density*, *Phys. Rev.* **D 74** (2006) 083514 [hep-ph/0605016] [INSPIRE].

[36] A. Arbey and F. Mahmoudi, *SUSY constraints from relic density: High sensitivity to pre-BBN expansion rate*, *Phys. Lett.* **B 669** (2008) 46 [arXiv:0803.0741] [INSPIRE].

[37] A. Arbey and F. Mahmoudi, *SUSY Constraints, Relic Density and Very Early Universe*, *JHEP* **05** (2010) 051 [arXiv:0906.0368] [INSPIRE].

[38] S. Lola, C. Pallis and E. Tzelati, *Tracking Quintessence and Cold Dark Matter Candidates*, *JCAP* **11** (2009) 017 [arXiv:0907.2941] [INSPIRE].

[39] M. Drees and F. Hajkarim, *Dark Matter Production in an Early Matter Dominated Era*, *JCAP* **02** (2018) 057 [arXiv:1711.05007] [INSPIRE].

[40] F. D'Eramo, N. Fernandez and S. Profumo, *When the Universe Expands Too Fast: Relentless Dark Matter*, *JCAP* **05** (2017) 012 [arXiv:1703.04793] [INSPIRE].

[41] M. Hindmarsh and O. Philipsen, *WIMP dark matter and the QCD equation of state*, *Phys. Rev.* **D 71** (2005) 087302 [hep-ph/0501232] [INSPIRE].

[42] M. Drees, F. Hajkarim and E.R. Schmitz, *The Effects of QCD Equation of State on the Relic Density of WIMP Dark Matter*, *JCAP* **06** (2015) 025 [arXiv:1503.03513] [INSPIRE].

[43] P. Gondolo and G. Gelmini, *Cosmic abundances of stable particles: Improved analysis*, *Nucl. Phys.* **B 360** (1991) 145 [INSPIRE].

[44] J. Edsjo and P. Gondolo, *Neutralino relic density including coannihilations*, *Phys. Rev.* **D 56** (1997) 1879 [hep-ph/9704361] [INSPIRE].

[45] A. Arbey and F. Mahmoudi, *SuperIso Relic: A Program for calculating relic density and flavor physics observables in Supersymmetry*, *Comput. Phys. Commun.* **181** (2010) 1277 [arXiv:0906.0369] [INSPIRE].

[46] A. Arbey and F. Mahmoudi, *SuperIso Relic v3.0: A program for calculating relic density and flavour physics observables: Extension to NMSSM*, *Comput. Phys. Commun.* **182** (2011) 1582 [INSPIRE].

[47] A. Arbey, F. Mahmoudi and G. Robbins, *SuperIso Relic v4: A program for calculating dark matter and flavour physics observables in Supersymmetry*, arXiv:1806.11489 [INSPIRE].

[48] N. Baro, F. Boudjema and A. Semenov, *Full one-loop corrections to the relic density in the MSSM: A Few examples*, *Phys. Lett.* **B 660** (2008) 550 [arXiv:0710.1821] [INSPIRE].

JHEP10(2018)132

[49] J. Harz, B. Herrmann, M. Klasen, K. Kovarik and Q.L. Boulc'h, *Neutralino-stop coannihilation into electroweak gauge and Higgs bosons at one loop*, *Phys. Rev.* **D 87** (2013) 054031 [arXiv:1212.5241] [INSPIRE].

[50] A. Arbey, *AlterBBN: A program for calculating the BBN abundances of the elements in alternative cosmologies*, *Comput. Phys. Commun.* **183** (2012) 1822 [arXiv:1106.1363] [INSPIRE].

[51] A. Arbey, J. Auffinger, K.P. Hickerson and E.S. Jenssen, *AlterBBN v2: A public code for calculating Big-Bang nucleosynthesis constraints in alternative cosmologies*, arXiv:1806.11095 [INSPIRE].

[52] K. Jedamzik, *Big bang nucleosynthesis constraints on hadronically and electromagnetically decaying relic neutral particles*, *Phys. Rev.* **D 74** (2006) 103509 [hep-ph/0604251] [INSPIRE].

[53] R. Allahverdi and M. Drees, *Thermalization after inflation and production of massive stable particles*, *Phys. Rev.* **D 66** (2002) 063513 [hep-ph/0205246] [INSPIRE].

[54] K. Mukaida and M. Yamada, *Thermalization Process after Inflation and Effective Potential of Scalar Field*, *JCAP* **02** (2016) 003 [arXiv:1506.07661] [INSPIRE].

[55] E.W. Kolb and M.S. Turner, *The Early Universe*, *Front. Phys.* **69** (1990) 1 [INSPIRE].

[56] T. Barreiro, E.J. Copeland and N.J. Nunes, *Quintessence arising from exponential potentials*, *Phys. Rev.* **D 61** (2000) 127301 [astro-ph/9910214] [INSPIRE].

[57] J.A. Frieman, C.T. Hill, A. Stebbins and I. Waga, *Cosmology with ultralight pseudo Nambu-Goldstone bosons*, *Phys. Rev. Lett.* **75** (1995) 2077 [astro-ph/9505060] [INSPIRE].

[58] E. Bagnaschi et al., *Likelihood Analysis of the pMSSM11 in Light of LHC 13-TeV Data*, *Eur. Phys. J.* **C 78** (2018) 256 [arXiv:1710.11091] [INSPIRE].

[59] Muon g-2 collaboration, G.W. Bennett et al., *Final Report of the Muon E821 Anomalous Magnetic Moment Measurement at BNL*, *Phys. Rev.* **D 73** (2006) 072003 [hep-ex/0602035] [INSPIRE].

[60] PICO collaboration, C. Amole et al., *Dark Matter Search Results from the PICO-60 C_3F_8 Bubble Chamber*, *Phys. Rev. Lett.* **118** (2017) 251301 [arXiv:1702.07666] [INSPIRE].

[61] XENON collaboration, E. Aprile et al., *First Dark Matter Search Results from the XENON1T Experiment*, *Phys. Rev. Lett.* **119** (2017) 181301 [arXiv:1705.06655] [INSPIRE].

[62] PandaX-II collaboration, X. Cui et al., *Dark Matter Results From 54-Ton-Day Exposure of PandaX-II Experiment*, *Phys. Rev. Lett.* **119** (2017) 181302 [arXiv:1708.06917] [INSPIRE].

[63] B.C. Allanach, *SOFTSUSY: a program for calculating supersymmetric spectra*, *Comput. Phys. Commun.* **143** (2002) 305 [hep-ph/0104145] [INSPIRE].

[64] A. Arbey, M. Battaglia and F. Mahmoudi, *Implications of LHC Searches on SUSY Particle Spectra: The pMSSM Parameter Space with Neutralino Dark Matter*, *Eur. Phys. J.* **C 72** (2012) 1847 [arXiv:1110.3726] [INSPIRE].

[65] A. Arbey, M. Battaglia and F. Mahmoudi, *Constraints on the MSSM from the Higgs Sector: A pMSSM Study of Higgs Searches, $B_s^0 \to \mu^+\mu^-$ and Dark Matter Direct Detection*, *Eur. Phys. J.* **C 72** (2012) 1906 [arXiv:1112.3032] [INSPIRE].

[66] A. Arbey, M. Boudaud, F. Mahmoudi and G. Robbins, *Robustness of dark matter constraints and interplay with collider searches for New Physics*, *JHEP* **11** (2017) 132 [arXiv:1707.00426] [INSPIRE].

JHEP10(2018)132